energies

MDPI

Article

A Cycle Voltage Measurement Method and Application in Grounding Grids Fault Location

Fan Yang [1,*], Yongan Wang [1], Manling Dong [2], Xiaokuo Kou [2], Degui Yao [2], Xing Li [1], Bing Gao [1] and Irfan Ullah [1]

[1] State Key Laboratory of Power Transmission Equipment & System Security and New Technology, Chongqing University, Chongqing 400044, China; wangyongancqu@126.com (Y.W.); lx918star@163.com (X.L.); gaobing.cqu@gmail.com (B.G.); Irfan.ee@cqu.edu.cn (I.U.)

[2] State Grid Henan Electric Power Corporation Research Institute, Zhengzhou 450052, China; dongmanling0211@163.com (M.D.); koukuo@163.com (X.K.); dashuiweng@gmail.com (D.Y.)

* Correspondence: yangfancqu@gmail.com; Tel.: +86-023-6510-2434

Received: 17 October 2017; Accepted: 16 November 2017; Published: 21 November 2017

Abstract: The corrosion of grounding grids can result in a grounding accident of a power system, and much attentions has been concentrated on the method used to detect a corrosion fault in a grounding grid, in which the methods of voltage measurement and magnetic field measurement are usually used. In this paper, a cycle voltage measurement method and L-curve regularization method are proposed to locate the faults in grounding grids. The L-curve method was used to select the appropriate regularization parameter, which can effectively balance the error and stability of the solution to the inverse problem. The uncertainty of the solution due to the ill-posed problem in the inverse problem has been well-solved. Experiments were conducted in a laboratory with two network types. In addition, a field experiment was carried out in a 110-kV substation. Both of the results showed that the method can effectively locate a branch fault with a single branch and multiple branches in the grounding grids.

Keywords: cycle voltage measurement; grounding grids; fault location; L-curve regularization method; inverse problem

1. Introduction

Grounding grids in substations are the important security means for the safe operation of a power system [1–3]. The branch resistance will increase when they are broken due to the corrosion or fracture of welding spots. Usually, the high resistance makes it harder for lightning current to disperse along the grounding grids into the earth, resulting in a reduction of security and reliability in operation. Therefore, calculating the branch resistance of grounding grids and locating the fault can allow us to effectively analyze the status of ground grids to avoid major accidents.

The traditional method of detecting a grounding grid is to inject a high current into the grid with the power system shut down and measure the relevant parameters, including ground impedance, earth potential rise, maximal touch potential difference and potential difference [4–6]. Once the performance is founded to be, there will be an excavation test. To some degree, the method cannot evaluate the performance of every single branch clearly. There are other kinds of solution for fault diagnosis in grounding grids, such as electrochemical method [7], the transient electromagnetic method [8,9], a frequency-domain analysis [10], the electromagnetic method [11–13], and the electric network method [14–17] for nondestructive testing.

Among the above methods, the electromagnetic method and the electric network method are mainly applied to calculate the branch resistance of grounding grids by regarding the grounding grid as a real resistance network to evaluate the status of the ground resistance. The idea of electromagnetic

theory is to inject a current into the grid along the down-lead wire and measure the magnitude and distribution of surface magnetic field, which is induced by the injected current. Both the broken point position and the status of the grounding can be obtained by analyzing the characteristics of the magnetic field [13]. This method also can detect the topology of the grounding grids [18,19]. The main problem of this method is how to accurately measure the induced magnetic field in the complex environment of the substation. In the electric network method, a fault diagnosis equation is established to detect a broken fault branch of grounding grids [15]. Liu et al. [17] has verified the effect on the result of fault location by the migration of the down-lead and the change of topology. Faleiro et al. [20] has studied the influence of an irregular surface of a multi-layered soil on ground resistance. However, solving the fault diagnosis equation will produce the ill-posed problem, and it will be unable to provide the exact solution for fault diagnosis. The key of electric network theory method is how to solve the inverse problem [14].

For the sake of solving the ill-posed problem, a branch broken fault location method of grounding grids based on cycle voltage measurement and L-curve regularization is proposed in this paper. The measurement method can be applied without shutting the power down, which is appropriate for evaluating grounding grids. The key idea of the regularization method is to constrain the objective function by adding a penalty factor to the error equation, which is usually used in image processing and forecasting short-term power production [21,22]. In this article, a fault diagnosis equation for grounding grids is put forward by a theoretical analysis and a 16-channel cycle measurement device is introduced. By applying the device and a regularized iterative algorithm on the detection of grounding grids, a mathematical model of fault diagnosis can be worked out. Finally, the feasibility and accuracy of the proposed method are verified by both laboratory and field experiments.

2. Methodology

2.1. Establishment of Fault Diagnosis Equation

For a model of a grounding grid with N nodes and B branches, the entire grounding grid can be regarded as a real resistance network, ignoring the inductance, capacitance, and mutual coupling between each branch since the current is small and direct. The dispersion of the injected current is not considered. The equivalent figure of the grounding grid is shown in Figure 1.

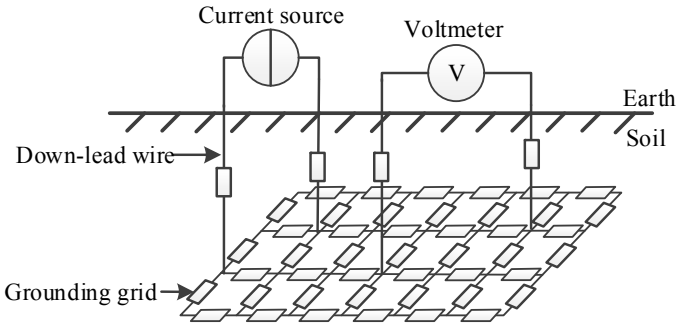

Figure 1. Equivalent schematic of the grounding grid.

The following equations are given below according to the electrical network theory method and the model of the grounding grid established above.

$$\boldsymbol{Y}_n \boldsymbol{U}_n = \boldsymbol{I}_n \tag{1}$$

$$\boldsymbol{A}\boldsymbol{Y}_b\boldsymbol{A}^{\mathrm{T}} = \boldsymbol{Y}_n \tag{2}$$

$$\boldsymbol{A}^{\mathrm{T}}\boldsymbol{U}_n = \boldsymbol{U}_b \tag{3}$$

$$\boldsymbol{Y}_b \boldsymbol{U}_b = \boldsymbol{I}_b \tag{4}$$

$$\boldsymbol{Y}_b = \begin{bmatrix} \frac{1}{R_1} & 0 & \cdots & 0 \\ 0 & \frac{1}{R_2} & \cdots & \vdots \\ \vdots & \vdots & \ddots & 0 \\ 0 & \cdots & 0 & \frac{1}{R_B} \end{bmatrix} \tag{5}$$

where $\boldsymbol{A}$ is the incidence matrix of the network; $\boldsymbol{Y}_b$ is the branch-admittance matrix; $\boldsymbol{Y}_n$ is the node-admittance matrix; $\boldsymbol{U}_b$ is the branch-voltage matrix; $\boldsymbol{U}_n$ is the node-voltage matrix; $\boldsymbol{I}_n$ is the node-current matrix; $\boldsymbol{I}_b$ is the branch-current matrix; and $\boldsymbol{R}$ is the branch-resistance matrix.

In order to calculate the grounding resistance of the grounding grid after years of corrosion, the node-voltage part from the grounding grid is measured when direct current (DC) is injected into the conductor along the down-lead wires. Assuming that $\boldsymbol{U}_{n0}$ is the measured value of the node-voltage and $\boldsymbol{U}_n(\boldsymbol{R})$ is the calculated value, the branch resistance R remains unknown yet. As the number of accessible node-voltages is far less than the number of branches, this results in the number of unknowns being greater than the number of equations, which is the so-called underdetermined equation. Hence, it is necessary to find an iterative equation to calculate the ground resistance. For a real resistance network with unknown branch resistance, theoretically, by minimizing $f(\boldsymbol{R})$, the branch resistance and its variation can be obtained when it is in accordance with the measured value. As a matter of fact, the measured value and the calculated value cannot be exactly equal due to the inverse problem, so the least square solution is established as follows:

$$\min f(\boldsymbol{R}) = \frac{1}{2}\|\boldsymbol{U}_n(\boldsymbol{R}) - \boldsymbol{U}_{n0}\|^2, \boldsymbol{R} = [R_1, R_2, \cdots, R_B]^{\mathrm{T}} \tag{6}$$

The optimal solution of each branch resistance can be obtained when the solution of Equation (6) is at minimum. The original designed resistance of the branch can be calculated according to the length, cross-sectional area, and electric resistivity of the galvanized steel strap which is the material of most grounding grids in China. As the resistance of each branch is calculated, the state of corrosion can be analyzed by comparing the calculated resistance of the branches with their initial values to achieve the purpose of branch fault location. Since the calculated value of the branch resistance cannot equal to the real value as same because the number of the measured value is far less than the number needed, this results in the ill-posed problem. Considering that, this article minimized the errors between them by the L-curve regularization method. The derivation of the Newton-Raphson algorithm can be obtained by the least square method as follows:

$$\frac{\partial f}{\partial \boldsymbol{R}} = [\boldsymbol{U}_n(\boldsymbol{R}) - \boldsymbol{U}_{n0}]\frac{\partial \boldsymbol{U}_n(\boldsymbol{R})}{\partial \boldsymbol{R}} = 0 \tag{7}$$

The series of Taylor of (6) at $\boldsymbol{R}(k)$ is as follows:

$$f(\boldsymbol{R}) = f(\boldsymbol{R}^{(k)}) + \frac{\partial f}{\partial \boldsymbol{R}}(\boldsymbol{R}^{(k)})(\boldsymbol{R} - \boldsymbol{R}^{(k)}) + \frac{1}{2}(\boldsymbol{R} - \boldsymbol{R}^{(k)})^{\mathrm{T}}\frac{\partial^2 f}{\partial \boldsymbol{R}^2}(\boldsymbol{R}^{(k)})(\boldsymbol{R} - \boldsymbol{R}^{(k)}) \tag{8}$$

Calculate the extreme point of (8):

$$\frac{\partial f}{\partial \boldsymbol{R}}(\boldsymbol{R}^{(k+1)}) = \frac{\partial f}{\partial \boldsymbol{R}}(\boldsymbol{R}^{(k)}) + (\boldsymbol{R}^{(k+1)} - \boldsymbol{R}^{(k)})^{\mathrm{T}}\frac{\partial^2 f}{\partial \boldsymbol{R}^2}(\boldsymbol{R}^{(k)}) = 0 \tag{9}$$

If $\frac{\partial^2 f}{\partial \boldsymbol{R}^2}(\boldsymbol{R}^{(k)})$ is reversible, then

$$\boldsymbol{R}^{(k+1)} = \boldsymbol{R}^{(k)} - \left(\frac{\partial^2 f}{\partial \boldsymbol{R}^2}(\boldsymbol{R}^{(k)})\right)^{-1}\left(\frac{\partial f}{\partial \boldsymbol{R}}(\boldsymbol{R}^{(k)})\right)^{\mathrm{T}} \tag{10}$$

Ignoring the higher-order terms, then

$$\frac{\partial^2 f}{\partial \boldsymbol{R}^2}(\boldsymbol{R}^{(\mathrm{k})}) = 2\left(\frac{\partial \boldsymbol{U}_n}{\partial \boldsymbol{R}}(\boldsymbol{R}^{(\mathrm{k})})\right)^{\mathrm{T}} \boldsymbol{U}_n(\boldsymbol{R}^{(\mathrm{k})}) \tag{11}$$

Take the derivative of (6) at $\boldsymbol{R}(k)$:

$$\frac{\partial f}{\partial \boldsymbol{R}}(\boldsymbol{R}^{(k)}) = 2\left(\frac{\partial \boldsymbol{U}_n}{\partial \boldsymbol{R}}(\boldsymbol{R}^{(k)})\right)^{\mathrm{T}} \left(\boldsymbol{U}_n(\boldsymbol{R}^{(k)}) - \boldsymbol{U}_{n0}\right) \tag{12}$$

Thus,

$$\boldsymbol{R}^{(k+1)} = \boldsymbol{R}^{(k)} - \left(\boldsymbol{J}_k^{\mathrm{T}} \boldsymbol{J}_k\right)^{-1} \boldsymbol{J}_k^{\mathrm{T}} \left(\boldsymbol{U}_n(\boldsymbol{R}^{(k)}) - \boldsymbol{U}_{n0}\right) \tag{13}$$

where $\boldsymbol{J}_k = \frac{\partial \boldsymbol{U}_n}{\partial \boldsymbol{R}}(\boldsymbol{R}^{(k)})$ is a Jacobi matrix.

Equation (13) is the Newton-Raphson (NR) algorithm iterative equation of the fault diagnosis equation. Nevertheless, an investigator who uses the NR algorithm alone will be unable to solve grounding grid fault diagnosis equation easily. The calculation of a Jacobi matrix is complex because of its morbidity, resulting in heavy computation in practice. Consequently, the resistance of branch needs to be calculated iteratively to be converged which may not be achieved when the initial value of the resistance is set inappropriately.

The regularization method is often used to improve the morbidity of the reconstruction process, which can stabilize the astringency of the solution.

2.2. The Tikhonov Regularization and the L-Curve Method

The forward and inverse problems of the fault diagnosis equation can be presented as follows:

Forward problem: $\boldsymbol{Y}_b \xrightarrow{\boldsymbol{I}_b} \boldsymbol{U}_b$.

Inverse problem: $\boldsymbol{U}_b \xrightarrow{\boldsymbol{I}_b^{-1}} \boldsymbol{Y}_b$.

The under determinedness of the inverse problem can be described as Figure 2.

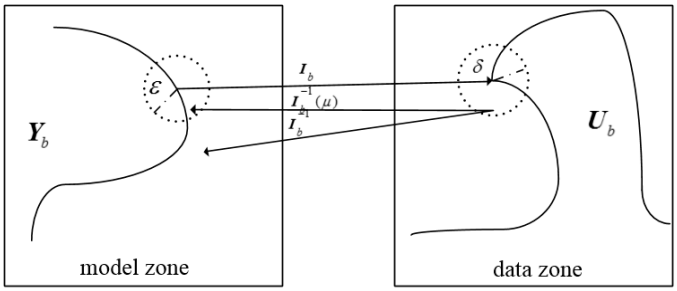

Figure 2. The under-determinedness of the inverse problem.

For the Equation (4), the number of node-voltages is far less than the number of branches, so the Jacobi matrix $\boldsymbol{J}_k$ is non-singular matrix, reflecting the underdeterminedness of the inverse problem. If the operators $\boldsymbol{Y}_b$ and $\boldsymbol{I}_b$ are known, solving $\boldsymbol{U}_b$ is the forward problem; otherwise, when $\boldsymbol{U}_b$ and $\boldsymbol{I}_b$ are given, the solution of $\boldsymbol{Y}_b$ may not be determined by $\boldsymbol{U}_b$ only, named the inverse problem. The condition number of the Jacobi matrix $\boldsymbol{J}_k$ is large, resulting in a larger condition number of the matrix $\boldsymbol{J}_k^{\mathrm{T}} \boldsymbol{J}_k$ in the process of solving the inverse problem, hence the solution of the inverse matrix cannot be obtained accurately. The process for solving the inverse problem needs to be optimized because of the high degree of morbidity when looking for the numerical solution. Ultimately, it comes down to a problem of optimization. There will be a significant large deviation from the real value when simply using the

least squares method. Considering that, the Tikhonov regularization iteration method is applied in order to reduce the error due to the sickness.

The Tikhonov regularization algorithm, which is a common regularization algorithm, can achieve a damping effect on the solution by adding a penalty function to the objective function. It can more than stabilize the solution, and also ensure the spatial resolution of the solution to a certain extent. We can add a constraint (penalty function) to the least squares target to achieve the purpose of improving the stability of the solution in the Tikhonov regularization method. The penalty function is added to the original objective function to obtain a new objective function, as follows:

$$f(\boldsymbol{x}) = \left|\left|\boldsymbol{T}_n(\boldsymbol{x}) - \boldsymbol{T}_{n0}\right|\right|^2 + \mu\left|\left|\boldsymbol{L}\cdot(\boldsymbol{x}-\boldsymbol{x}_0)\right|\right|^2 \tag{14}$$

where $\boldsymbol{x}$ is the desired variable, $\boldsymbol{T}_n(\boldsymbol{x})$ is the equation about $\boldsymbol{x}$, $\boldsymbol{T}_{n0}$ is the final iterative target, μ is the regularization parameter, and $\boldsymbol{L}$ is the matrix of regularization.

Aiming at the objective function, a new iterative equation can be obtained by Newton-Raphson algorithm:

$$\boldsymbol{x}^{(k+1)} = \boldsymbol{x}^{(k)} - \left(\boldsymbol{J}_k^{\mathrm{T}}\boldsymbol{J}_k + \mu\boldsymbol{L}^{\mathrm{T}}\boldsymbol{L}\right)^{-1}\cdot\left[\boldsymbol{J}_k^{\mathrm{T}}\cdot\left(\boldsymbol{T}_n(\boldsymbol{x}^{(k)}) - \boldsymbol{T}_{n0}\right) - \mu\boldsymbol{L}^{\mathrm{T}}\boldsymbol{L}\cdot(\boldsymbol{x}^{(k)} - \boldsymbol{x}^{(0)})\right] \tag{15}$$

where $\boldsymbol{J}$ is the Jacobian matrix of $\boldsymbol{x}$.

The inverse problem of solving matrix $\boldsymbol{J}_k^{\mathrm{T}}\boldsymbol{J}_k$ in the Newton-Raphson algorithm can be converted into solving matrix $(\boldsymbol{J}_k^{\mathrm{T}}\boldsymbol{J}_k + \mu\boldsymbol{L}^{\mathrm{T}}\boldsymbol{L})$ through regularization. The value of μ keeps changing to adjust the eigenvalue of the matrix in the process of iteration process, which is beneficial for meeting the requirement of matrix inversion.

The selection of regularization parameter μ is vital for the calculation's result. For the ill-posed problem, the smaller μ is, the closer the results are to the real value. Nonetheless, the stability of the solution is better when the parameters should be bigger. So the parameter needs to be selected properly to make both the regularization solution $||\boldsymbol{L}\cdot(\boldsymbol{x}-\boldsymbol{x}_0)||$ and the residual term $||\boldsymbol{T}_n(\boldsymbol{x}) - \boldsymbol{T}_{n0}||$ smaller. In this research, the regularization parameter is selected by the L-curve method.

The L-curve is made up of the regularization solution and the residual term with parameter variation in the logarithmic scale. The characteristic of the L-curve is that the scale curve is presented clearly as a capitalized "L". The curve of the horizontal part is mainly dominated by the regularization error (μ is selected too big), while the curve of the vertical part is mainly dominated by the error of $\boldsymbol{T}_{n0}$ (μ is selected too small). Hanke et al. [23] take the maximum curvature position (L-corner) on the curve as the inflection point, whose corresponding parameter μ is regarded as the appropriate regularization parameter.

If,

$$\rho = \lg(||\boldsymbol{T}_n(\boldsymbol{x}) - \boldsymbol{T}_{n0}||) \tag{16}$$

$$\theta = \lg(||\boldsymbol{L}\cdot(\boldsymbol{x}-\boldsymbol{x}_0)||) \tag{17}$$

Since the regularization parameter is continuous in the Tikhonov regularization, the L-curve is smooth and twice differentiable. So the curvature function $c(\mu)$ about parameter μ can be defined as follows:

$$c(\mu) = \frac{\rho'\theta'' - \rho''\theta'}{\left[(\rho')^2 + (\theta')^2\right]^{\frac{3}{2}}} \tag{18}$$

As the curvature $c(\mu)$ is maximum, the corresponding point is the L-corner. The selection of the regularization parameter can be converted to the calculation of the L-corner, which is easier and more intuitive by a numerical analysis.

2.3. The Calculation of the Branch Resistance by L-Curve Regularization

Applying the regularization algorithm on the equation of fault location for grounding grids, Equations (14) and (15) can be materialized as follows:

$$f(\boldsymbol{R}) = \frac{1}{2}\|\boldsymbol{U}_n(\boldsymbol{R}) - \boldsymbol{U}_{n0}\|^2 + \frac{1}{2}\mu\|\boldsymbol{L}(\boldsymbol{R})\|^2 \tag{19}$$

$$\boldsymbol{R}^{(k+1)} = \boldsymbol{R}^{(k)} - \left(\boldsymbol{J}_k^{\mathrm{T}}\boldsymbol{J}_k + \mu\boldsymbol{L}^{\mathrm{T}}\boldsymbol{L}\right)^{-1} \cdot \left[\boldsymbol{J}_k^{\mathrm{T}} \cdot \left(\boldsymbol{U}_n(\boldsymbol{R}^{(k)}) - \boldsymbol{U}_{n0}\right) + \mu\boldsymbol{L}^{\mathrm{T}}\boldsymbol{L} \cdot (\boldsymbol{R}^{(k)} - \boldsymbol{R}^{(0)})\right] \tag{20}$$

where, $\frac{1}{2}\mu\|\boldsymbol{L}(\boldsymbol{R})\|^2$ is the regularization term, and μ is regularization parameter. Equation (19) is the fault diagnosis function of grounding grids based on regularization. Each branch resistance R can be obtained by solving (20) with the standard Tikhonov regularization iteration method, which is given below:

$$\begin{cases} \boldsymbol{p}^{(k)} = -[\boldsymbol{J}^{\mathrm{T}}(\boldsymbol{R}^{(k)})\boldsymbol{J}(\boldsymbol{R}^{(k)}) + \mu_k\boldsymbol{E}]^{-1}\boldsymbol{J}^{\mathrm{T}}(\boldsymbol{R}^{(k)})[\boldsymbol{U}_n(\boldsymbol{R}^{(k)}) - \boldsymbol{U}_{n0}] \\ \boldsymbol{R}^{(k+1)} = \boldsymbol{R}^{(k)} + \boldsymbol{p}^{(k)} \end{cases} \tag{21}$$

where $\mu_k\boldsymbol{E}$ is the regularization term, $\boldsymbol{E}$ is the unit matrix, and μ_k is regularization parameter. The selection method is carried out by the L-curve method, whose initial value is $\boldsymbol{R}^{(0)} = [R_{10}, R_{20}, \cdots, R_{B0}]^{\mathrm{T}}$, and $\boldsymbol{J}(\boldsymbol{R})$ is the Jacobian matrix of $f(\boldsymbol{R})$.

$$\boldsymbol{J}(\boldsymbol{R}) = \begin{bmatrix} \frac{\partial \boldsymbol{U}_1(\boldsymbol{R})}{\partial R_1} & \cdots & \frac{\partial \boldsymbol{U}_1(\boldsymbol{R})}{\partial R_B} \\ \vdots & \ddots & \vdots \\ \frac{\partial \boldsymbol{U}_N(\boldsymbol{R})}{\partial R_1} & \cdots & \frac{\partial \boldsymbol{U}_N(\boldsymbol{R})}{\partial R_B} \end{bmatrix} \tag{22}$$

Calculate the Jacobian matrix as follows

$$\frac{\partial \boldsymbol{I}_n}{\partial \boldsymbol{R}_i} = \frac{\partial(\boldsymbol{Y}_n\boldsymbol{U}_n)}{\partial \boldsymbol{R}_i} = 0 \tag{23}$$

$$\frac{\partial \boldsymbol{U}_n}{\partial R_i} = -\boldsymbol{Y}_n^{-1}\frac{\partial \boldsymbol{Y}_n}{\partial R_i}\boldsymbol{U}_n \tag{24}$$

Through Equation (21), solve Equation (19) and the actual value of the grounding grid can be obtained.

The flow diagram for fault location in a grounding grid based on the Tikhonov regularization algorithm is shown in the Figure 3. The algorithm flow is as follows.

(1) Set $k = 0$ and the accuracy ε. The initial value is selected as the branch resistance under normal conditions, $\boldsymbol{R}^{(0)} = [R_{10}, R_{20}, \cdots, R_{B0}]^{\mathrm{T}}$.
(2) Calculate the Jacobian matrix $\boldsymbol{J}(\boldsymbol{R})$ and choose the regularization parameter μ_k from the L-curve method.
(3) Calculate the iteration step size $\boldsymbol{P}^{(k)}$.
(4) Calculate $\boldsymbol{R}^{(k+1)} = \boldsymbol{R}^{(k)} + \boldsymbol{P}^{(k)}$ and the iteration error $\varepsilon^{(k+1)} = \|\boldsymbol{U}_n(\boldsymbol{R}^{(k+1)}) - \boldsymbol{U}_n(\boldsymbol{R}^{(k)})\|$. If $\varepsilon^{(k+1)} < \varepsilon$, let $\boldsymbol{R} = \boldsymbol{R}^{(k+1)}$; otherwise, make $k = k + 1$, and turn towards step (2).
(5) Export the optimal solution $\boldsymbol{R}$.

Through the solution method mentioned above, the value of the resistance of a grounding grid branch is calculated. Correspondingly, the corrosion status of the grounding grids can be graded easily. The feasibility and accuracy of the proposed method are verified by experiments below.

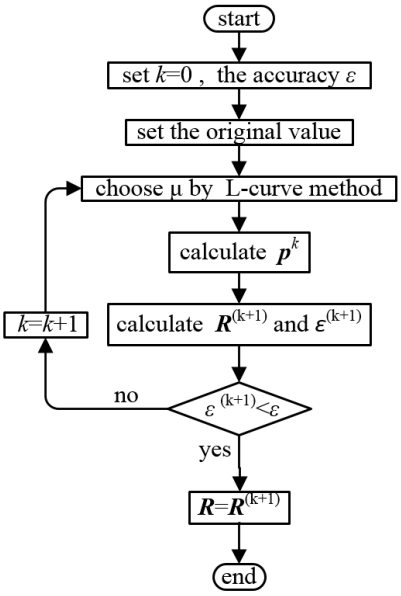

Figure 3. The calculation flow chart.

The initial branch resistance can be calculated accurately based on the design drawing. In addition, there is only a small part of the branches in the grounding grids where corrosion exists. At the same time, the resistance of the corroded branches is generally 1 to 10 times greater than the normal branches. Therefore, the initial values are close to the objective solution in the data set of the solution space, which is extremely helpful for the convergence of the iterative calculation. A broken branch in the solution space is reflected as an extreme point. The iteration step size from the initial value to the extreme point is greater than the initial value to the value of the corroded branch, which means that the iteration speed is faster and it is more easily converged at the extreme point. Consequently, the success of the solution sought can be guaranteed with a precise initial value and an appropriate threshold value.

2.4. Principle of Cycle Voltage Measurement

To solve Equation (19), massive data on the node-voltage must be obtained. However, there are a limited number of accessible down-lead wires to obtain the corresponding data. Consequently, a 16-channel cycle voltage measurement method [15] is used to gain enough potential data with limited accessible down-lead wires.

We choose 16 accessible down-lead wires from the grounding grids to be the current channels f inflow and outflow, which are represented by N1, N2, . . . , N16. First of all, we maintain the N1 as the outflow node while change the inflow node from N2 to N16 in turn. We measure the voltage of the other 14 nodes when the DC current of 1A is injected into the inflow node and extract current from the outflow node at every turn. After the inflow node is N16, we change the outflow node to be N2 and the inflow node to be N3 to N16 in turn, repeat the steps above until N15 is the outflow node and N16 is the inflow node. The process can be described as follows:

i = 1, N1 is the outflow node, N2, N3, . . . , N16 is the inflow node in turn;
i = 2, N2 is the outflow node, N3, N3, . . . , N16 is the inflow node in turn;
. . . . . .
i = 15, N15 is the outflow node, N16 is the inflow node.

Without changing the position of the wire, there are 120 sets of node-voltage in once measurement. The workload is greatly reduced with the massive data measured. The mode of cycle measurement is as shown in Figure 4.

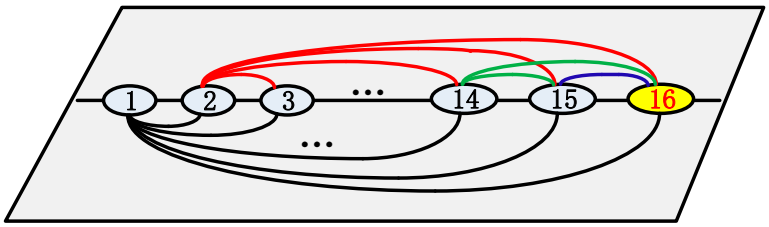

Figure 4. Mode of cycle measurement.

There will be 14 valid node-voltage data in a set of measurements. In addition, N16 is chosen to be the common zero potential reference node, hence there are 120 × 13 = 1560 node-voltage data can be used for the calculation through a single measurement with 16 down-lead wires.

For field measurements, 16 down-lead wires are not always necessary; it depends on the size of the grid. The length of each wire used to connect the device and the down-lead wire is 25 m, which means that a circle with a radius of 25 m can be covered in a single measurement. A regional measurement method is used when the area of the grid is out of the scope [24]. For the small grounding grids, the number of channels can be changed from 4 to 16 when the number of the accessible down-lead wires is less than 16.

A 24-bit analog to digital conversion chip is used to a measurement's accuracy. The effective resolution of the chip is $1/(2^{19}-1)$, which can completely satisfy the requirement of measurement. The switch of the 16-channel is managed by ADG1206 (Analog Devices, Norwood, MA, USA) to ensure the stability of the system. The DC current of 1A is generated by an Advanced RISC Machine (ARM) microcontroller STM32F103ZET6 (STMicroelectronics, Geneva, Switzerland), which is the major chip of the device. The structure of the channel switch module is shown Figure 5.

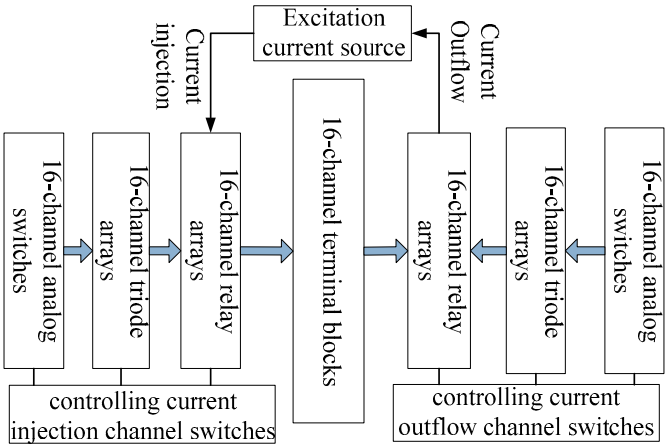

Figure 5. Channel switch module.

There is a positive feedback circuit in the excitation current source module to make sure that the error of the output current is less than 0.15%. The output current curve is shown in Figure 6 when the resistance load is 1 Ω. Normally, the resistance of a grounding grid is usually in the range of 50 mΩ to 500 mΩ.

The system must have a specific load capacity to deal with the different conditions of the grounding grids. The test diagram is shown in Figure 7 and results of different load tests are shown in Table 1.

The load test of the device shows that the output current can remain stable when the load varies between 0.05 Ω and 20 Ω, which corresponds with the actual situation of the grounding grid.

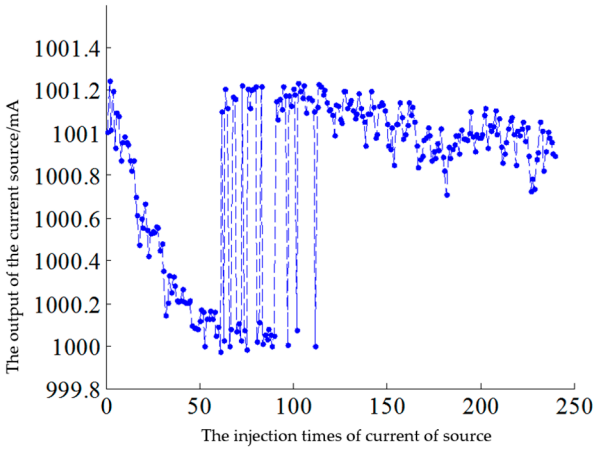

Figure 6. The output current test curve with 1 Ω.

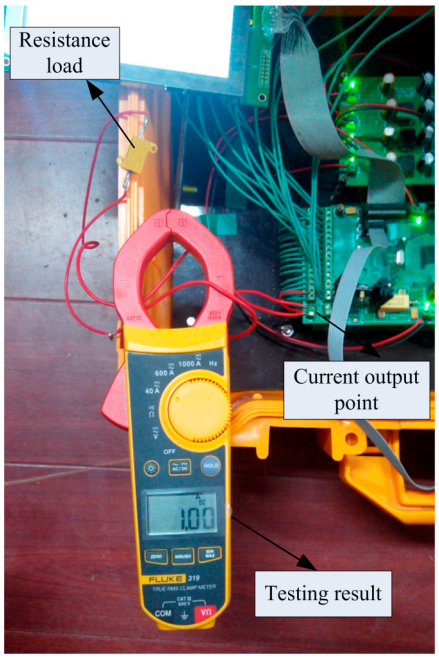

Figure 7. The diagram of resistance load capacity test.

Table 1. The output current result of the different load test.

The Value of Load/Ω	0.05	0.1	0.5	1.0	5.0	10.0	20.0	30.0	40.0
The Output Current/A	1.00	1.00	1.00	1.00	1.00	1.00	1.00	0.99	0.99

To verify the accuracy of the measuring device, a simulation model that was the same as the network in the laboratory was built in MATLAB (R2012a), shown in Figure 8. The branch of a grounding grid is made by highly precise resistors of 1 Ω. The simulation diagram and the positions of the 16-channel are as follows. The results of the measurement and simulation are shown in Table 2.

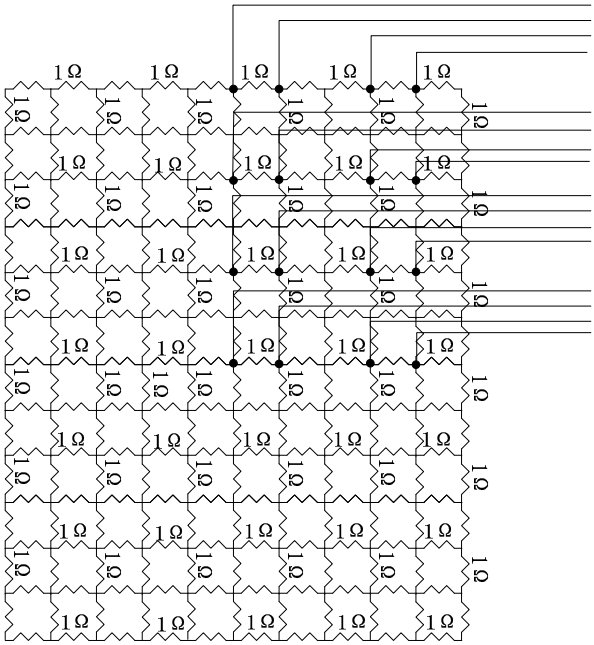

Figure 8. The simulation resistance network in MATLAB.

Table 2. The part results of the measurement and simulation.

Measured Data by Device (mV)	Simulation Data by MATLAB (mV)	Measurement Error (mV)	Percentage Error (%)
237.80	237.76	0.04	0.0168%
257.52	254.32	3.20	1.260%
246.67	245.10	1.57	0.641%
252.83	252.20	0.63	0.250%
251.11	250.13	0.98	0.392%
258.61	257.92	0.69	0.268%
258.99	256.23	2.66	1.040%
245.94	245.13	0.81	0.330%
251.38	250.63	0.75	0.300%
...	...	...	...

The results of the test between measurement and simulation shows that the percentage error of the measurement is less than 1.3%, which is appropriate for the fault diagnosis equation established above.

3. Experiments and Discussion

Based on the analysis above, this paper proposes a method to locate the broken fault branches of grounding grids with regularization method. To decrease the measurement workload and obtain more node-voltage data, in this section we use a 16-channel cycle voltage measurement device and verify the effect of locating the faults by the method proposed.

3.1. Lab Tests

Based on the theory of an electric network, two models were built with highly precise resistors and galvanized steel strap in the laboratory.

3.1.1. Tests with Precise Resistor

A branch of a grounding grid is made by highly precise resistors of 1 Ω. The schematic and actual diagrams of the model are shown in Figure 9.

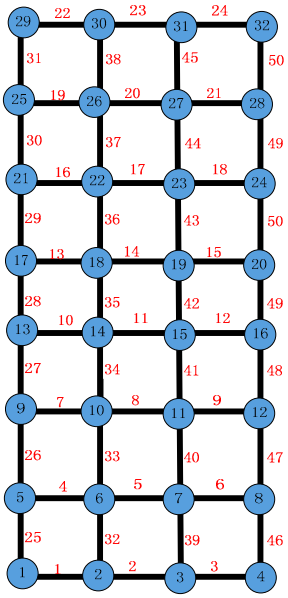

Figure 9. The schematic and actual diagrams of the model made by precise resistors.

Two types of simulation cases were used to verify the feasibility of the algorithm: a single branch fault with one branch faulted and multiple faults with three branches faulted. These two cases can represent most of the real fault conditions. To identify the fault quickly, the ordinate was set as the magnification times of the branch resistance, and the abscissa is the serial number of the branch.

- Case of a broken single branch

By replacing the corresponding resistor, the 20th branch of the network in Figure 9 was set to 5 Ω, 10 Ω, and broken to simulate the corresponding situation in corrosion. First, we injected a DC current of 1 A from one node and extracted it out from another node and then measured the node-voltage with the 16-channel cycle voltage measurement device in different cases. After processing the data with the diagnosis program, the results are shown in Figure 10:

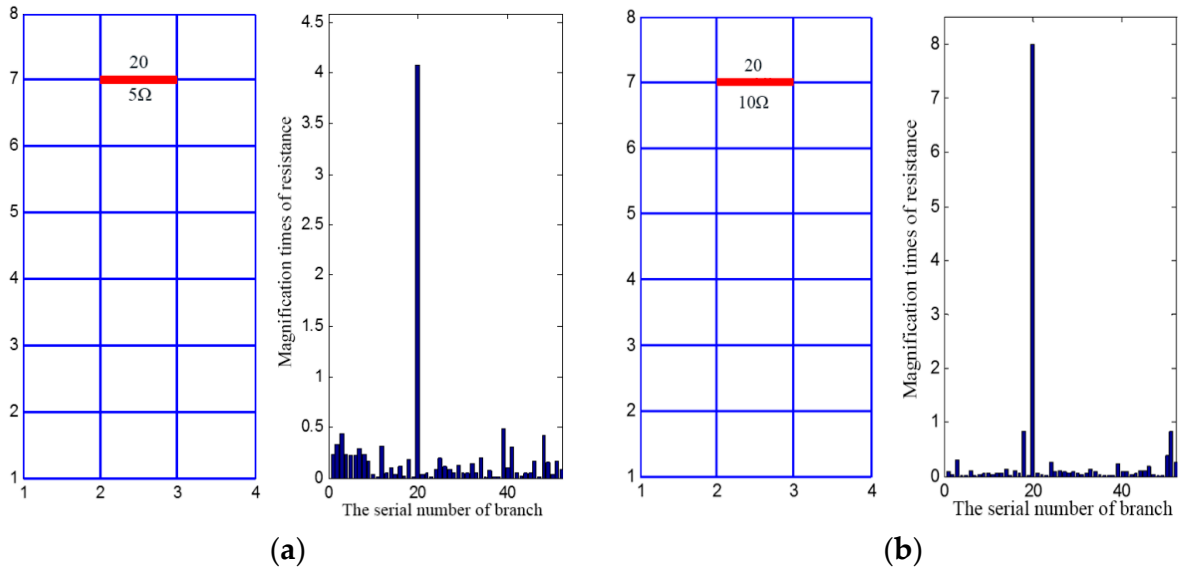

Figure 10. *Cont.*

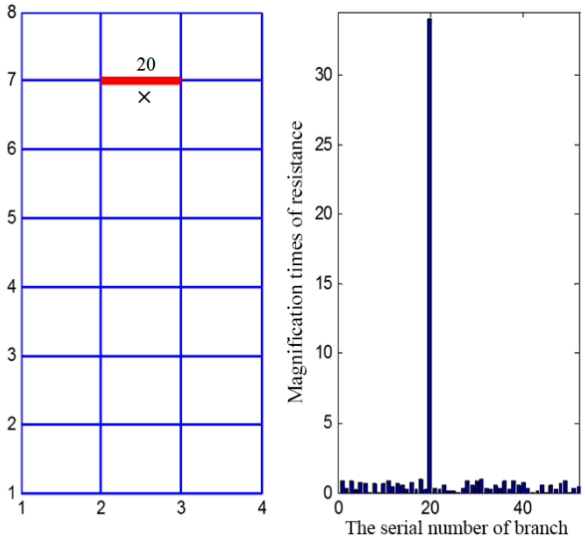

(**c**)

Figure 10. The results of the single branch fault case with a real resistance network. (**a**) The resistance of the fault branch was 5 Ω; (**b**) The resistance of the fault branch was 10 Ω; (**c**) The fault branch was broken.

The results of the diagnosis showed that the 20th branch was 4 times, 9 times, and 35 times greater than the normal value respectively, which meant that the resistance was 5 Ω, 10 Ω, and 36 Ω. As the magnification times are more than 10 times, this means that the branch is broken. The results were confirmed in the practical situation.

- Case of multiple broken branches

Furthermore, the 20th, 42nd and 33rd were set as fault branches to verify the accuracy of the diagnosis. The three branches were set to 5 Ω, 10 Ω, and broken to simulate the various degrees of corrosion. Here is the result of the diagnosis program as shown in Figure 11.

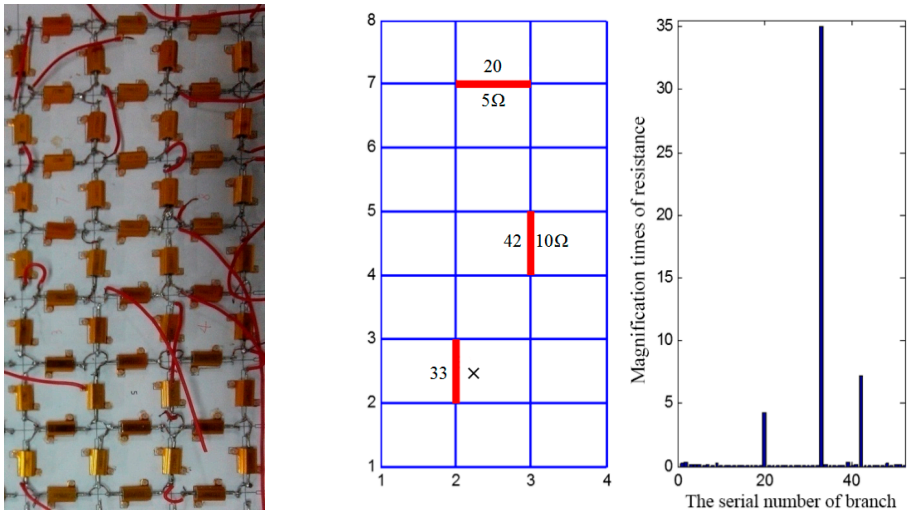

(**a**) (**b**)

Figure 11. The results of the multiple branch fault case with a real resistance network. (**a**) Resistance network; (**b**) Diagnosis result.

The results of the diagnosis showed that the 20th branch was 4 times, the 42nd branch was 8 times, and the 33rd branch was 35 times greater than the average value, respectively, which meant that the resistance was 5 Ω, 9 Ω, and 36 Ω. As the magnification times are more than 10 times, this means that the branch is broken. The results were confirmed in the practical situation with a reasonable error. The result also showed that the resistance of branches can still be calculated accurately as the fault appeared simultaneously.

3.1.2. Tests with Galvanized Steel Strap

The real resistance model is made of highly precise resistors, which is different from real grounding grids. To simulate grounding grids in the real field, an 8 m × 4 m experimental model shown in Figure 12 was established in the laboratory. The model is made of galvanized steel strap, which is the same material as real grounding grids and buried in the soil. The branch resistance is 0.525 mΩ and it can be broken as needed to simulate the situation of a broken fault in grounding grids. In the experiment, we selected the 4th, 6th, 11th, 14th, 17th, 23rd, 28th, and 30th nodes in the network as the measurement nodes, and a DC current of 1 A is injected from one node and extracted out from the another node. The inflow and outflow nodes consist of six pairs of the above measurement nodes. At the same time, we measured the rest of the node-voltage by using the 16-channel measurement device. So, the branch resistance of grounding grids can be calculated according to the regularization method proposed in this paper. The current excitation nodes selected are shown in Table 3.

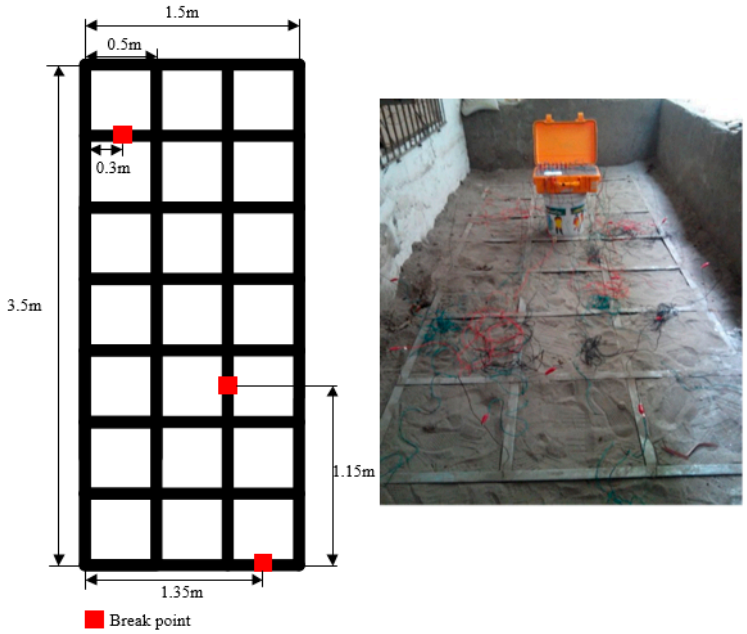

Figure 12. The schematic and actual diagrams of the model made of galvanized steel strap.

Table 3. The pair of exciting current nodes.

Number	1	2	3	4	5	6
Inflow Node	4	11	6	14	23	30
Outflow Node	23	17	28	30	6	17

- Case of a single broken branch

When the 19th branch is broken, which is the simulation of the case of a single branch fault, we selected the current excitation node by Table 3 to inject 1 A direct current and measure the other

node-voltages. The branch resistance calculated with the data processed by the regularization method. The results are shown in Figure 13.

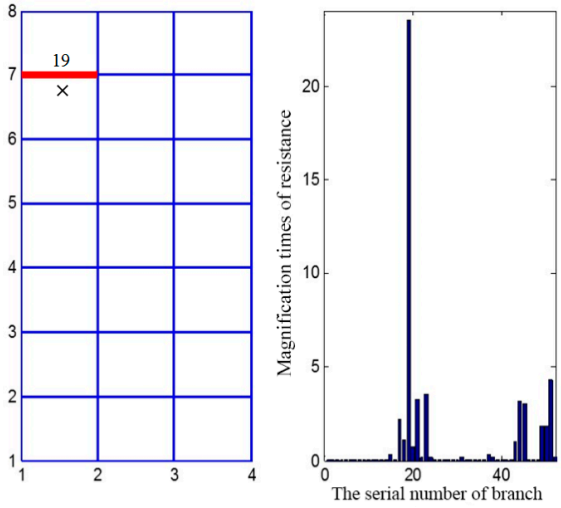

Figure 13. The results of the single branch fault case with the galvanized steel strap network.

- Case of multiple broken branches

To simulate the case of multiple faults, the 3rd, 19th, and 41st branches were broken in the laboratory experiment.

The remaining node-voltage were measured while injecting the 1 A of direct current into the current injection node circularly with the 16-channel cycle voltage measurement device. The results of the calculation are as shown in Figure 14. When the 19th branch is broken, it indicates that the branch resistance is 35 times greater than the normal value, while the other three broken branches are more than 19 times greater. The results also show that the grounding grid fault diagnostic program can locate both a single branch fault and multiple branch faults available with an obvious effect.

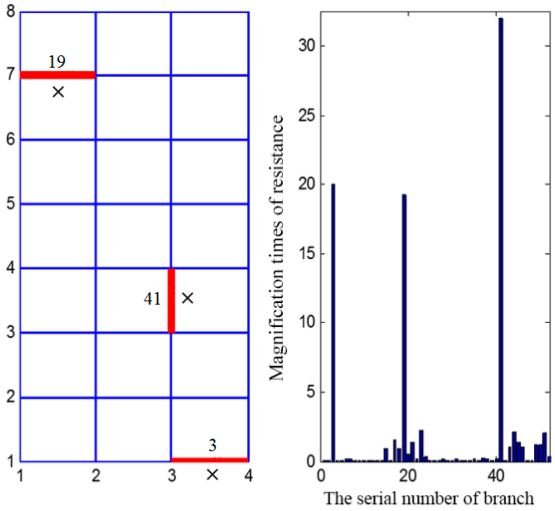

Figure 14. The results of the multiple branch faults case with the galvanized steel strap network.

The experimental results with the experiment platform that is made of galvanized steel strap show that the algorithm can accurately calculate the disconnection fault condition of different cases, to achieve the purpose of locating a disconnection fault in a grounding grid.

3.2. Field Tests

To verify the accuracy of the algorithm, a 110-kV substation was selected for an experimental analysis. The structure of a grounding grid with 35 nodes, 43 branches, and buried 0.8 m deep in the substation is shown in Figure 15. The circle stands for the grounding grid's node number, while the line stands for the branch number. As shown in Figure 16, in the experiment, the fault of the grounding grid was set artificially, which means that the 17th branch was broken. In Figure 15, a direct current of 1 A is injected from the node which is selected from Table 4, and the rest of the node-voltages were measured by using the 16-channel device. The situation of the grounding grid is shown in Figure 16.

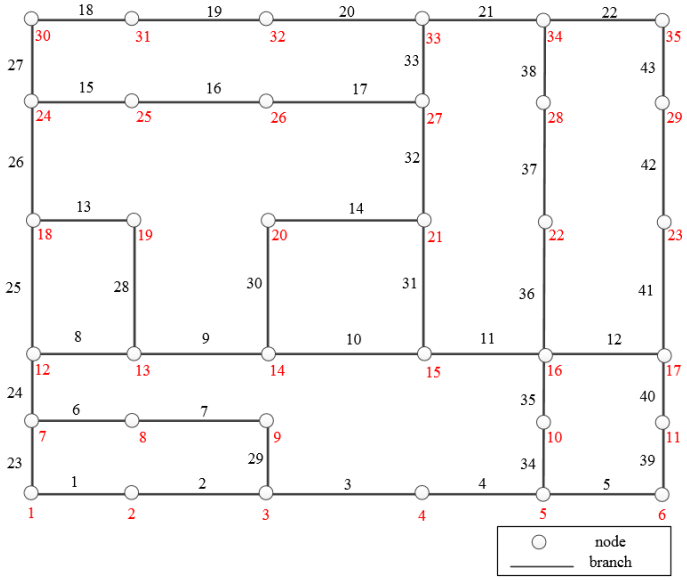

Figure 15. The model of the substation grounding grid.

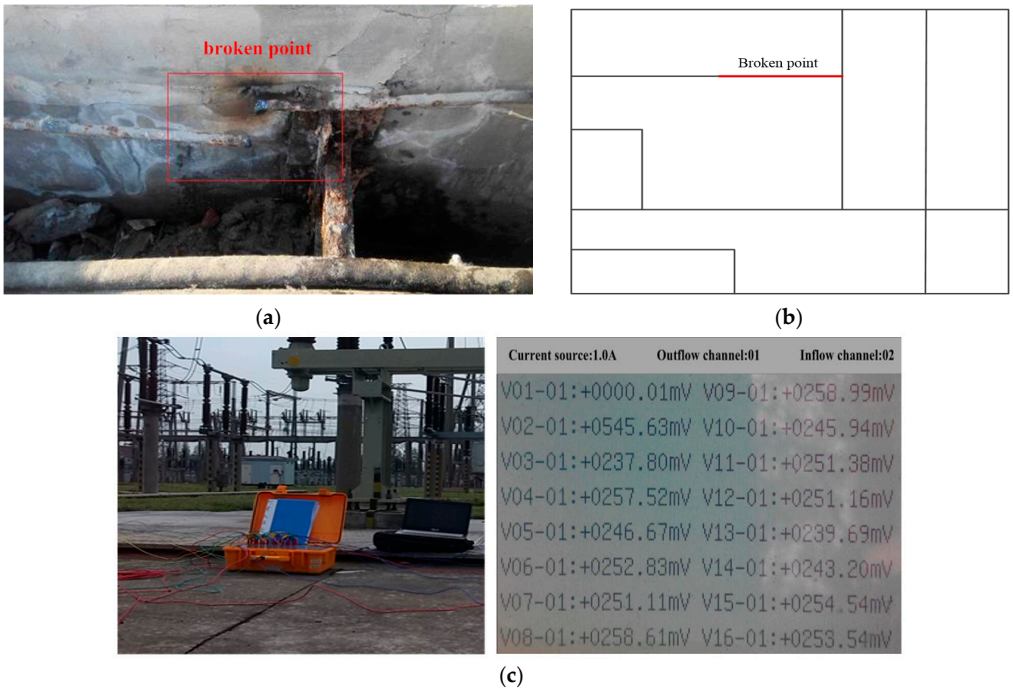

Figure 16. The field experiment. (**a**) The scene photo; (**b**) The model diagram; (**c**) The process of diagnosis.

Table 4. The pair of exciting current nodes.

Number	1	2	3	4	5	6
Inflow Node	2	7	9	18	28	31
Outflow Node	28	24	31	28	7	9

We input the relevant parameters of the grounding grid and the measured data into the diagnostic program, and the results obtained from the calculation are shown in Figure 17.

The results showed that resistance of the 15th, 16th, and 17th branches increases by more than 30 times while the magnification times of the others are less than 5 times. It can be seen intuitively that the resistance value of these three branches has a more significant change than the resistance of the remaining branches. Hence, these three branches need to be emphasized. Figure 17 shows that the proposed algorithm based on the L-curve regularization method can calculate the changes of branch resistance in the ground accurately. The magnification times of the resistance can reflect the status of grounding grids to efficiently locate the branch faults of grounding grids in the real field. This method can not only locate the branch faults in the grounding grids of a substation, but also reflect a certain degree of grounding network branch corrosion according to the increase in the branch resistance.

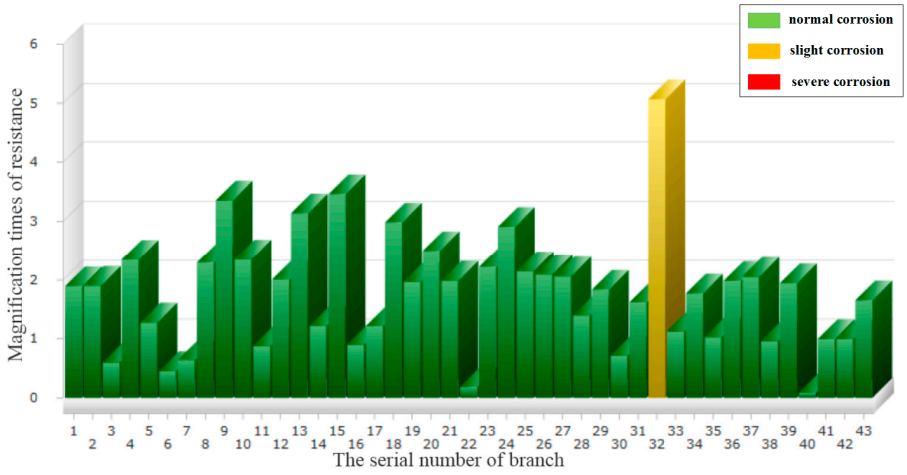

(**a**)

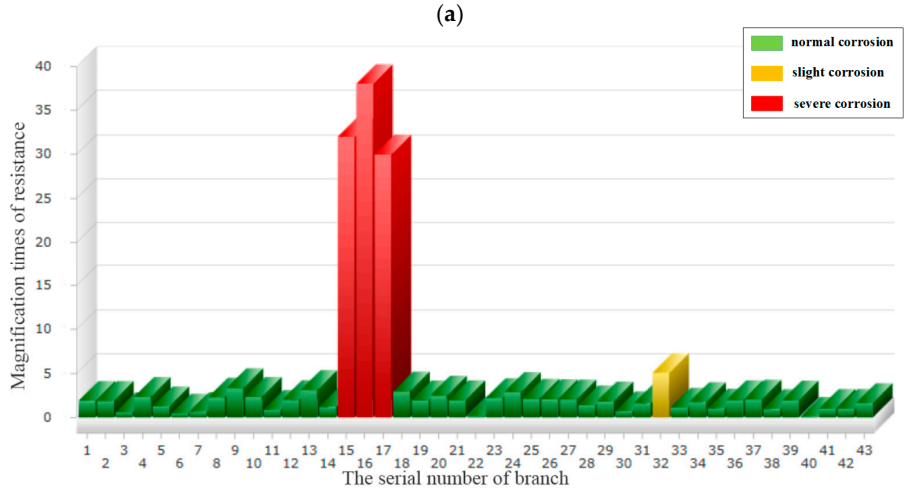

(**b**)

Figure 17. The result in the field experiment. (**a**) The result of pre-fault; (**b**) The result of post-fault.

4. Conclusions

A new branch fault location method for grounding grids based on a 16-channel cycle voltage measurement method and L-curve regularization is proposed. By measuring the node-voltage with the device and adding a penalty function to the objective function with the L-curve method, the damping effect of the solution is achieved. Finally, the underdeterminedness that is generated by solving the inverse problem in fault diagnosis is worked out. The results of experiments in the laboratory with two models show that location algorithm can locate different cases of branch faults accurately. The result of a field experiment in a 110-kV substation indicates that the location algorithm can effectively detect a branch fault of a grounding grid in a complicated environment.

The proposed method can not only locate a branch fault but can also evaluate the performance of a grounding grid to ensure the safety of the substation. Furthermore, this is a convenient method because the equipment still can be running without shutting down the while system when the method is applied. The parameters such as different soil resistivity, multilayer soil, and the dispersion of current are not considered in the paper. Therefore, we would study on this issue in future work.

Acknowledgments: This work was supported by National Natural Science Foundation of China (Grant No. 51477013).

Author Contributions: All the authors contributed equally to all the sections of this work.

Conflicts of Interest: The authors declare no conflict of interest.

References

1. Asimakopoulou, F.E.; Tsekouras, G.J.; Gonos, I.F.; Stathopulos, I.A. Estimation of seasonal variation of ground resistance using artificial neural networks. *Electr. Power Syst. Res.* **2013**, *94*, 113–121. [CrossRef]
2. Alipio, R.; Schroeder, M.A.O.; Afonso, M.M. Voltage Distribution Along Earth Grounding Grids Subjected to Lightning Currents. *IEEE Trans. Ind. Appl.* **2015**, *51*, 4912–4916. [CrossRef]
3. IEEE PES Substations Committee. *IEEE Guide for Safety in AC Substation Grounding*; IEEE Standard 80-2000; IEEE: Washington, DC, USA, 2000.
4. Long, X.; Dong, M.; Xu, W.; Li, Y.W. Online monitoring of substation grounding grid conditions using touch and step voltage sensors. *IEEE Trans. Smart Grid* **2012**, *3*, 761–769. [CrossRef]
5. Kostić, V.I.; Raičević, N.B. A study on high-voltage substation ground grid integrity measurement. *Electr. Power Syst. Res.* **2016**, *131*, 31–40. [CrossRef]
6. Sverak, J.G.; Dick, W.K.; Dodds, T.H.; Heppe, R.H. Safe substation grounding-part I. *IEEE Trans. Ind. Appl.* **1981**, *100*, 4281–4290. [CrossRef]
7. Zhang, X.L.; Luo, P.; Mo, N.; Wang, Y.G.; Li, Y.L. Development and application of electrochemical detection system for grounding grid corrosion state. *Proc. CSEE* **2008**, *28*, 152–156.
8. Dommel, H.W. Digital computer solution of electromagnetic transients in single-and multiphase networks. *IEEE Trans. Power Appar. Syst.* **1969**, *PAS-88*, 388–399. [CrossRef]
9. Yu, C.; Fu, Z.; Wang, Q.; Tai, H.M.; Qin, S. A novel method for fault diagnosis of grounding grids. *IEEE Trans. Ind. Appl.* **2015**, *51*, 5182–5188. [CrossRef]
10. Zhang, P.H.; He, J.J.; Zhang, D.D.; Wu, L.M. A fault diagnosis method for substation grounding grid based on the square-wave frequency domain model. *Metrol. Meas. Syst.* **2012**, *19*, 63–72. [CrossRef]
11. Dawalibi, F. Electromagnetic fields generated by overhead and buried short conductors. Part 2—Ground networks. *IEEE Power Eng. Rev.* **1986**, *6*, 33–34. [CrossRef]
12. Heimbach, M.; Grcev, L.D. Grounding system analysis in transients programs applying electromagnetic field approach. *IEEE Trans. Power Deliv.* **1997**, *12*, 186–193. [CrossRef]
13. Zhang, B.; Zhao, Z.; Cui, X.; Li, L. Diagnosis of breaks in substation's grounding grid by using the electromagnetic method. *IEEE Trans. Magn.* **2002**, *38*, 473–476. [CrossRef]
14. Yang, F.; Jiang, Y.; Shi, Q.; Chen, T.; He, W. Magnetic field inverse problem of grounding grid and its application. *Int. J. Appl. Electromagn.* **2012**, *40*, 173–183.

15. Liu, K.; Yang, F.; Wang, X.; Gao, B.; Kou, X.; Dong, M.; Jadoon, A. A novel resistance network node potential measurement method and application in grounding grids corrosion diagnosis. *Prog. Electromagn. Res. M* **2016**, *52*, 9–20. [CrossRef]
16. Zeng, J.; Lin, S.; Xu, Z. Sparse solution of underdetermined linear equations via adaptively iterative thresholding. *Signal Process.* **2014**, *97*, 152–161. [CrossRef]
17. Liu, J.; Ni, Y.-F.; Lu, W.; Wang, S.; Li, Z.-Z. Influence of touchable nodes deviation on grounding grids corrosion diagnosis and its correction. *High Volt. Eng.* **2008**, *34*, 2349–2354.
18. Wang, X.; He, W.; Yang, F.; Zhu, L.; Liu, X. Topology detection of grounding grids based on derivative method. *Trans. China Electrotech. Soc.* **2015**, *30*, 73–78, 89.
19. Li, C.; He, W.; Yao, D.; Yang, F.; Kou, X.; Wang, X. Topological measurement and characterization of substation grounding grids based on derivative method. *Int. J. Electr. Power Energy Syst.* **2014**, *63*, 158–164.
20. Faleiro, E.; Asensio, G.; Moreno, J. An estimate of the uncertainty in the grounding resistance of electrodes buried in two-layered soils with non-flat surface. *Energies* **2017**, *10*, 176. [CrossRef]
21. Huang, W.; Xiao, L.; Liu, H.; Wei, Z. Hyperspectral imagery super-resolution by compressive sensing inspired dictionary learning and spatial-spectral regularization. *Sensors* **2015**, *15*, 2041. [CrossRef] [PubMed]
22. Li, G.; Li, B.J.; Yu, X.G.; Cheng, C.T. Echo state network with bayesian regularization for forecasting short-term power production of small hydropower plants. *Energies* **2015**, *8*, 12228–12241. [CrossRef]
23. Hanke, M.; Longman Scientific Technical. *Conjugate Gradient Type Methods for Ill-Posed Problems*; John Wiley & Sons, Inc.: New York, NY, USA, 1995.
24. Liu, J.; Ni, F.; Wang, Q.; Li, Z.; Wang, S. Grounding grids corrosion diagnosis using a block dividing approach. *High Volt. Eng.* **2011**, *37*, 1194–1202.